

12-Tungstophosphoric acid niched in Zr-based metal-organic framework: a stable and efficient catalyst for Friedel-Crafts acylation

Latif Ullah^{1,2}, Guoying Zhao^{1*}, Zichen Xu¹, Hongyan He¹,
Muhammad Usman^{1,3} & Suojiang Zhang^{1*}

¹Beijing Key Laboratory of Ionic Liquids Clean Process, Key Laboratory of Green Process Engineering, State Key Laboratory of Multiphase Complex Systems, Institute of Process Engineering, Chinese Academy of Sciences, Beijing 100190, China;

²University of Chinese Academy of Sciences, Beijing 100049, China;

³Center of Excellence in Nanotechnology, King Fahd University of Petroleum and Minerals, Dhahran 3126, Saudi Arabia

Received August 7, 2017; accepted November 20, 2017; published online March 2, 2018

Heteropolyacids (HPA) are well known for their versatile solid acid catalysis in diverse chemical reactions, however they suffer from low surface area (<10 m²/g) and leaching into the reactions media, which reduce their prospects as industrial catalyst. Herein, a novel hybrid material HPW@Zr-BTC, composed of 12-tungstophosphoric acid (HPW) and Zr^{IV}-benzene tri-carboxylate (Zr-BTC) metal-organic framework (MOF), was prepared via one-pot solvothermal method. Excellent HPW loading up to 32.3 wt% was achieved, and HPW@Zr-BTC composite proved to be highly stable, besides the crystalline morphology of Zr-BTC was intact. The catalytic activity of the hybrid composite was explored via Friedel-Crafts acylation of anisole with benzoyl chloride. The 28.2 wt% HPW@Zr-BTC showed excellent catalytic performance, with 99.4% anisole conversion and 97.6% yield (*p*-methoxybenzophenone) under solvent free conditions. Excellent retention of catalytic activity was achieved after at least five consecutive runs due to non-observable HPW leaching. The promising activity and stability of the catalyst forecasted its potential industrial applications.

dodeca-tungstophosphoric acid, Zr-BTC, metal-organic frameworks, one-pot solvothermal synthesis, heterogeneous catalysis, anisole acylation, high temperature XRD

Citation: Ullah L, Zhao G, Xu Z, He H, Usman M, Zhang S. 12-Tungstophosphoric acid niched in Zr-based metal-organic framework: a stable and efficient catalyst for Friedel-Crafts acylation. *Sci China Chem*, 2018, 61, <https://doi.org/10.1007/s11426-017-9182-0>

1 Introduction

In chemical transformations, such as petroleum refining and fine chemicals production [1,2], solid acid catalysts play a vital role to lower the process cost and check environmental problems of homogeneous acid catalysts. In this regard, heteropolyacids (HPA) because of their strong and versatile solid acid nature, been applied in multiple chemical processes [1,3–5]. Amongst the heteropolyacids, 12-tung-

stophoric acid (HPW) is the strongest and most stable solid acid reported [1]. HPW has successfully been applied to catalyze a number of chemical processes [6–9], like oxidation [10–12], formalin dimerization [1], Friedel-Crafts (FC) reactions [13,14], and formic acid degradation [15]. However, leaching in reaction media and low surface area (<10 m²/g) hinder their way to industrial application. One approach to address these shortcomings is to access the HPW-based heterogeneous catalysis, by supporting/encapsulating heteropolyacids on/inside a porous matrix such as silica [16], carbon [17], MCM-41 [18], and porous zir-

*Corresponding authors (email: gyzhao@ipe.ac.cn; sjzhang@ipe.ac.cn)

conia [19,20]. Hitherto, because of the low surface area and small pore volume of such conventional porous supports, only a limited amount of HPW could be loaded, besides leaching of the polyanions is still a problem.

Metal-organic frameworks (MOFs), are relatively new crystalline hybrid materials, known for their large surface area, ordered and tunable porosity, and low structure density [21–23]. The Cu and Cr-based MOFs have recently received much attention for heteropoly acids encapsulation [24–30]. Although fascinating results have been reported, even though the Cu and Cr-based MOFs are sensitive to aqueous and acidic media [31,32], Cr^{VI} is carcinogenic and is considered a highly unwanted pollutant (LTV level of 0.05 mg/L) in water. Therefore, it is imperative to find new hosts to support heteropoly acids, especially MOFs having large surface area and environmentally benign metal body that is resistant to corrosive solvents. Previously, ZrO₂ was used as support for HPW to catalyze Friedel-Crafts acylation [19], transesterification for biodiesel synthesis and glycerol valorisation [20]. Zirconium MOFs having large surface area, acid resistive properties, considerable thermal stability and environmentally hazard-free zirconium metal [33–36], have shown potential prospects in this regard. However, only a few studies have reported heteropoly acids supported in Zr-based MOFs [37,38]. It was perceived, that zirconium-based MOFs would be a good choice to allow high HPW loading and to suppress the polyanion leaching into the reaction media.

Zr-BTC was chosen for this study due to its large surface area (~2300 m²/g), good stability and pertinent porous structure [33]. Zr-BTC has two types of pores, as shown in Scheme 1. The smaller tetrahedral pores ~0.5–0.7 nm size, and the relatively larger adamantane type pores with internal diameter 1.8–2.0 nm, which were rationally a good choice to host the HPW moieties that have the size of ~1.2 nm [39].

Herein, we report the encapsulation of 12-tungstophosphoric acid [H₃PW₁₂O₄₀] in the porous Zr-BTC via one-pot solvothermal strategy, to prepare HPW@Zr-BTC hybrid materials, and onward explore its catalytic performance in Friedel-Crafts acylation of anisole with benzoyl chloride as a model acid catalyzed reaction. Friedel-Crafts acylation was

chosen because of its importance in organic transformations that include C–C bond coupling reactions [40]. Traditionally, FC acylation has been catalyzed homogeneously by H₂SO₄, HF or AlCl₃, which causes severe environmental problems, thus environmentally benign heterogeneous catalysts are greatly desired for such reactions [41–43]. To the best of our knowledge, this is the first attempt to encapsulate heteropoly acids into Zr-BTC, and explore its catalytic activity in acylation reactions.

2 Experimental

2.1 Preparation of Zr-BTC

Zr-BTC was synthesized following the method adopted from Furukawa *et al.* [44]. In a typical reaction, ZrOCl₂·8H₂O (6.46 g, 20 mmol) and trimesic acid (1.47 g, 7 mmol) linker were dissolved in (600 mL) pre-mixed solvent containing 50% *N,N*-dimethylformamide (DMF) and 50% formic acid in a gas tight glass bottle. Modulator benzoic acid 2 eqv. (based on Zr salt) was also added, as reported elsewhere [45]. The precursors were sonicated for 10 min followed by stirring at room temperature until no suspended particles were visible. The mixture was then placed in a pre-heated oven for two days at 120 °C. Zr substituted POMs have previously been reported for monolacunary POMs [46], for example in Dawson type POMs [47] forming [PW₁₁O₃₉Zr(μ-OH)₂]³⁻ and [Zr(α₂-P₂W₁₇O₆₁)₂]¹⁶⁻ monomeric complexes; neither was observed in this case. Upon completion of the reaction, the white crystals were thoroughly washed with fresh DMF, and then with acetone. The crystals were evacuated at 60 °C for 8 h, followed by activation at 110 °C for 6 h.

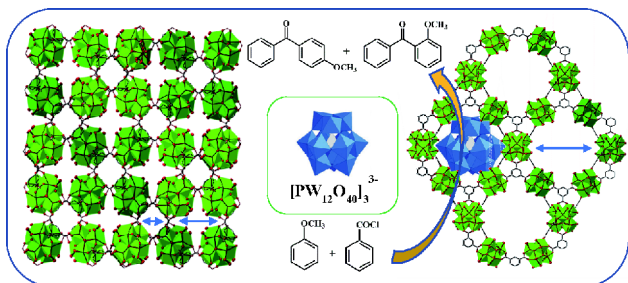
2.2 Preparation of HPW@Zr-BTC

Synthesis of the hybrid HPW@Zr-BTC was achieved following the same procedure as Zr-BTC, with the addition of 12-tungstophosphoric acid in the synthesis media. Different millimoles of 12-phosphotungstic acid (HPW) was added to the mixture of ZrOCl₂·8H₂O and BTC under constant stirring and variable loadings of the HPW were achieved (18.6 wt% to 32.3 wt%), as confirmed by inductively coupled plasma optical emission spectrometer (ICP-OES).

3 Results and discussion

3.1 Crystalline and morphological studies

The XRD patterns for the Zr-BTC pristine and its HPW encapsulated composites are shown in Figure 1. The XRD peaks obtained for pure Zr-BTC are in good agreement with the calculated MOF-808 type, corresponding to CCDC# 1002672 in the Cambridge Crystal Structural Database [44].



Scheme 1 Structure representation of Zr-BTC, dodeca-tungstophosphoric acid and anisole acylation reaction (color online).

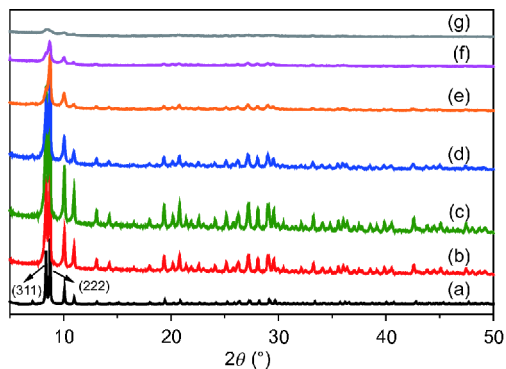


Figure 1 Powder XRD Bragg's peaks of Zr-BTC simulated (CCDC# 1002672) (a), Zr-BTC pristine (b), 18.6 wt% HPW@Zr-BTC (c), 25.2 wt% HPW@Zr-BTC (d), 28.2 wt% HPW@Zr-BTC (e), 32.3 wt% HPW@Zr-BTC (f) and >32.3 wt% HPW@Zr-BTC (g) (color online).

The two sharp peaks at the 8.36° (311) and 8.74° (222) for the pristine Zr-BTC revealed that the material obtained had high crystallinity. No separate ZrO_2 peaks were observed, which indicated good reproducibility of the MOF material. From the XRD patterns indicated in **Figure 1**, the addition of HPW up to (18.6 wt%) into the Zr-BTC revealed improved crystallinity, that could be due to the anionic templating effect of oxometallates; discussed elsewhere [30,48]. Also, it could be seen that further addition of HPW into the host hardly affected the crystalline morphology of the pristine Zr-BTC up to a threshold amount of HPW (25.2 wt% HPW@Zr-BTC). With further increase in the amount of HPW, the intensity of the representative peak at 8.36° (311) declined drastically, due to low pH of the medium [49,50], that protonated the linkers, inhibiting coordination with the metal. Additional HPW loading resulted in greatly damaging the Bragg's peaks of Zr-BTC, which was also verified from the scanning electron micrographs (SEM) shown in **Figure 2** (vide infra).

The SEM results (**Figure 2**) revealed the pristine Zr-BTC to possess well defined octahedral microcrystals having average crystal diameter of 200 nm. The micrographs suggested, that up to a certain limit HPW addition had little impact upon the crystals, but as the HPW content increased beyond 28.2 wt%, the crystal shape changed quickly towards distortion. This might be the result of low pH of the system which resulted in protonation of BTC, therefore inhibiting the coordinating ability of BTC, and leading to crystals shrinkage and ultimately crystal disappearance [49]. No polyanions agglomeration was observed, as evident from XRD (**Figure 1**) and energy dispersive spectrometer (EDS) elemental mapping (Figure S1, Supporting Information online), which showed well dispersed HPW inside the host framework.

3.2 FTIR spectroscopy

To confirm whether the HPW had been successfully encapsulated into the Zr-BTC, Fourier transform infrared spectroscopy (FTIR) studies were conducted. FTIR spectra for the bulk HPW, pristine Zr-BTC, and HPW@Zr-BTC samples are shown in **Figure 3**. The observed vibration bands between $1300\text{--}1750\text{ cm}^{-1}$, corresponding to the carboxylate linkers [37] of the pristine Zr-BTC were well maintained in the hybrid samples. Additionally, new peaks appeared in the region of $600\text{--}1200\text{ cm}^{-1}$ for the hybrid HPW@Zr-BTC composite samples, which were assigned to the P–O, W–O–W and W=O vibration bands in HPW [51]. The peaks at ν (cm^{-1}): 1050 (PO_4^-), 823, 881 and 942 (W–O–W) and 960 (W=O) cm^{-1} stretches were all in good agreement with the earlier works [49,50].

3.3 BET surface and textural studies

Table 1 summarizes the textural properties, such as BET

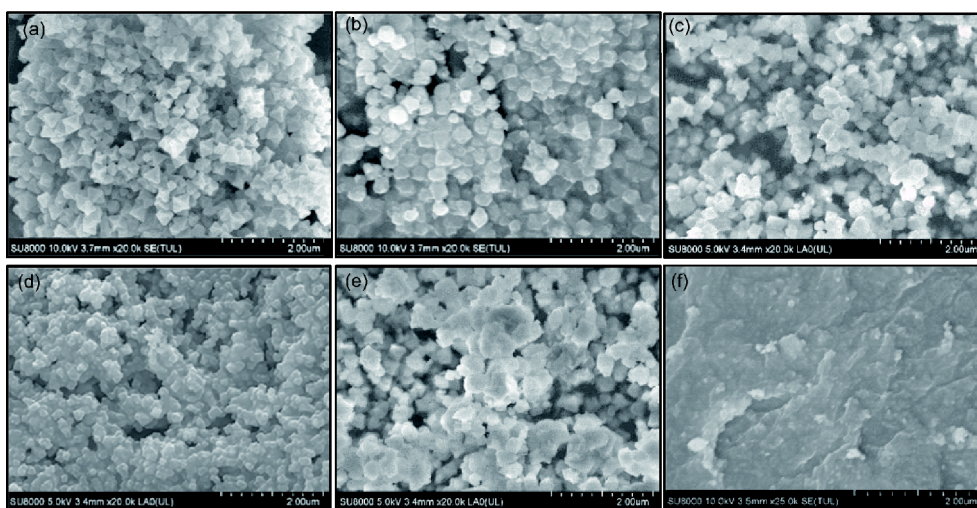


Figure 2 SEM micrographs of Zr-BTC pristine (a), HPW@Zr-BTC composites 18.6 wt% (b), HPW@Zr-BTC composites 25.2 wt% (c), HPW@Zr-BTC composites 28.2 wt% (d), HPW@Zr-BTC composites 32.3 wt% (e), and HPW@Zr-BTC composites >32.3 wt% (f).

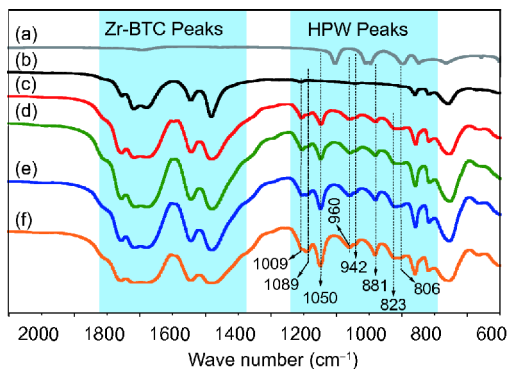


Figure 3 FTIR spectra for HPW bulk (a), Zr-BTC pristine (b), 18.6 wt% HPW@Zr-BTC (c), 25.2 wt% HPW@Zr-BTC (d), 28.2 wt% HPW@Zr-BTC (e), and 32.3 wt% HPW@Zr-BTC (f) (color online).

surface area and pore volume of pristine Zr-BTC and HPW@Zr-BTC composites. Consistent with the increase in HPW loadings, the surface area of the composite structures decreased from 2058.6 to 1065.6 m²/g. Figure 4(a) shows type-1 isotherms, which reveal the microporous nature of Zr-BTC with no associated capillary condensation. The isotherms for the HPW@Zr-BTC composites showed no observable sign of swelling, which confirmed that the pores were not damaged by HPW incorporation into the host assembly. Also the size of the micropores were not less than 0.5 nm, that might have inhibited the tensile strength amongst the adjacent pores to damage the pores integrity [52]. The pore size distribution of the materials was calculated from the desorption branch of the isotherm using Horvath-Kowazoe (HK) method, which revealed two types of micropores; smaller pores of 0.5–0.7 nm and larger pores of ~1.8 nm, in well agreement with the Ref. [33] (Figure 4 (b)). The larger pores of ~1.8 nm size in the Zr-BTC edifice were available to accept HPW, and upon the introduction of HPW their size decreased, whereas the smaller pores (~0.5–0.7 nm) remained almost unaffected, as shown in Figure 4(b).

3.4 XPS analysis

To understand the interaction of HPW with the host structure, X-ray photoelectron spectroscopy (XPS) studies were conducted and the behaviour of tungsten and phosphorus

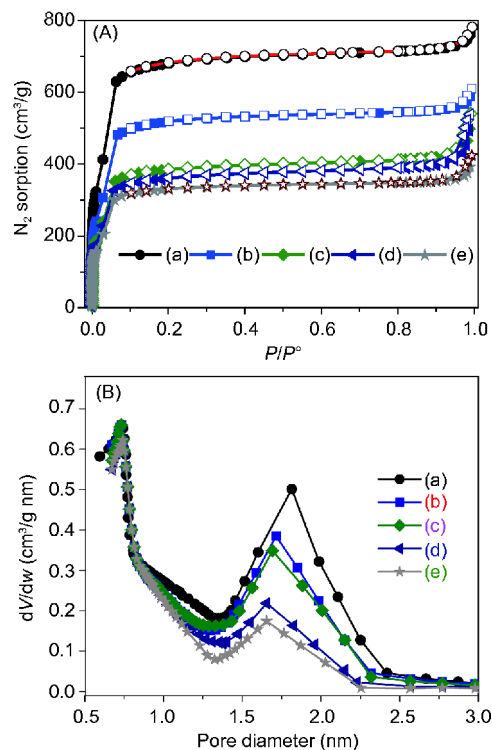


Figure 4 (A) BET sorption isotherms for Zr-BTC Pristine (a), 18.6 wt% HPW@Zr-BTC (b), 25.2 wt% HPW@Zr-BTC (c), 28.2 wt% HPW@Zr-BTC (d), and 32.3 wt% HPW@Zr-BTC (e). (B) Pore size distribution calculated from adsorption peak using Horvath-Kowazoe (HK) method (color online).

was observed, before and after encapsulation (Figure 5). For tungsten W⁶⁺ before encapsulation, two principal peaks were obtained at 35.70 and 37.75 eV corresponding to W 4f_{7/2} and W 4f_{5/2}, respectively. The peak ratio between them was about 4:3 which showed that the HPW was in its fully oxidized (W₃O and WO₂) state [53]. For the 28.2 wt% HPW@Zr-BTC, the tungsten peaks were almost of the same height and ratio but slightly shifted towards higher binding energies, with W4f_{7/2} and W4f_{5/2} peaks that appeared at 36.55 and 38.75 eV, corresponding to the stronger interaction of HPW with the host Zr-BTC [19]. In addition to these two peaks, another distinctive W⁴⁺ (W5P_{3/2}) peak at 42.60 eV was observed, which indicated the formation of WO₃ [53]. The phosphorus P 2p peaks for bulk HPW and encapsulated samples are also shown in Figure 5. The fundamental peaks

Table 1 Surface studies for the Zr-BTC pristine and the HPA@Zr-BTC samples

Entry	Sample type	Surface area (BET) (m ² /g)	Pore size (nm)	Pore volume (cm ³ /g) ^{a)}	HPW:Zr-BTC (wt%)
1	Zr-BTC (Pristine)	2058.6	1.814	1.432	0:100
2	18.6 wt% HPA@Zr-BTC	1633.6	1.713	1.195	18.6:81.4
3	25.2 wt% HPA@Zr-BTC	1284.5	1.691	1.114	25.2:74.8
4	28.2 wt% HPA@Zr-BTC	1117.7	1.654	0.993	28.2:71.8
5	32.3 wt% HPA@Zr-BTC	1065.6	1.653	0.765	32.3:67.7

a) Calculated by using Horvath-Kowazoe (HK) method.

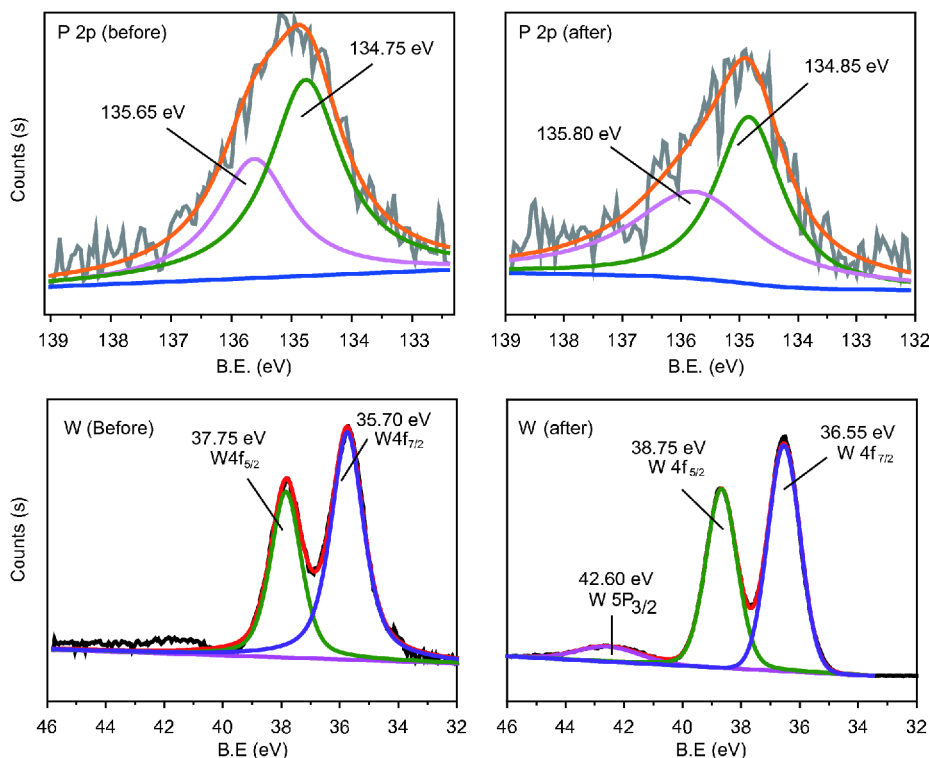


Figure 5 X-ray photoelectron spectra for phosphorus (P 2p) and tungsten (W 4f) of HPW, before and after encapsulation. Results for 28.2 wt% HPW@Zr-BTC (color online).

for phosphorous P $2p_{3/2}$ and P $2p_{1/2}$ in Keggin structure were observed at 134.75 and 135.65 eV, respectively, which were slightly shifted to 134.85 and 135.80 eV after encapsulation. The slight shift in binding energy for the phosphorus octahedra showed that the Keggin topology of the HPW was retained inside the MOF, yet it was interactive with the host matrix [19]. This was also corroborated by ^{31}P -NMR (Figure 8, *vide infra*).

3.5 TGA analysis

TGA studies were conducted to substantiate the thermal stability of the Zr-BTC and its corresponding HPW@Zr-BTC composites. From the thermographs in Figure 6, the bulk HPW followed one-stepped, whereas the pristine Zr-BTC and HPW@Zr-BTC composites followed two-stepped thermal degradation. The two-stepped thermal degradation is considered a typical feature for MOF materials as reported elsewhere [31,54]. The bulk HPW revealed weight loss at around 135 °C, mainly due to dehydration, and beyond that point there was no evident weight loss till 700 °C. For Zr-BTC, the observable and prolonged weight loss around 70 °C was obvious, due to the evaporation of embedded moisture and guest molecules. The second trough for the pristine Zr-BTC emerged at around 330 °C, which was referred to as linker sites opening and structure degradation [34]. The thermographs for the HPW@Zr-BTC composite

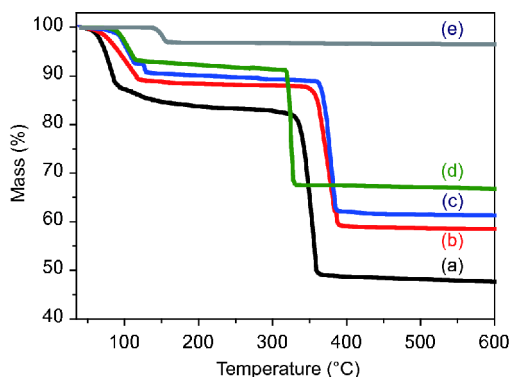


Figure 6 TGA thermographs for pristine Zr-BTC (a), 18.6 wt% HPW@Zr-BTC (b), 28.2 wt% HPW@Zr-BTC (c), 32.3 wt% HPW@Zr-BTC (d), and bulk HPW (e) (color online).

(18.26, 28.2 and 32.3 wt%) displayed less dehydration and guest removal as compared to the pristine Zr-BTC, indicating that HPW had occupied the free space previously available for the guest. For the 18.3 and 28.2 wt% HPW@Zr-BTC composites, the linker sites opening was delayed to 348 and 362 °C, respectively, showing enhancement in stability of the Zr-BTC after the introduction of heteropoly acids. TGA findings were corroborated by HT-XRD (high-temperature XRD) for 28 wt% HPW@Zr-BTC (Figure 7). The HT-XRD gave a detailed account of the phase behaviour of the material under investigation. It was apparent that the

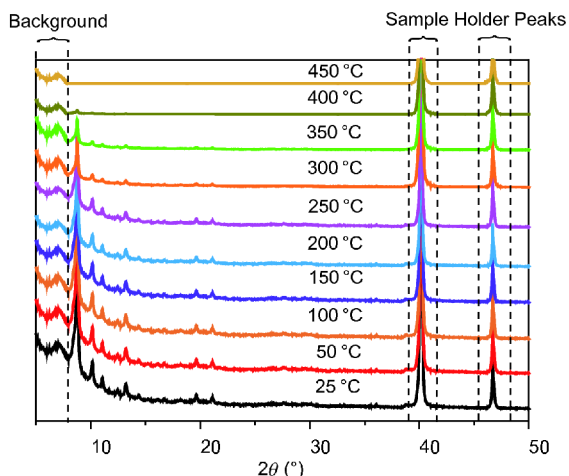


Figure 7 High temperature XRD for 28.2 wt% HPW@Zr-BTC (color online).

enhancement in the thermal stability of Zr-BTC by the incorporation of HPW, was due to the templating effect of heteropoly anions [31,48,55,56]. In contrast, the onset of the thermal degradation for 32.3 wt% HPW@Zr-BTC appeared earlier than for the pristine Zr-BTC, i.e., at 318 °C. Thus, it could be inferred that up to a certain limit the heteropoly anions stabilized the Zr-BTC structure, however as the amount of HPW exceeded this threshold value; the low pH of the medium protonated the BTC linker which consequently led to structure deterioration.

3.6 Solid state ^{31}P -NMR

Solid state ^{31}P -NMR was employed to understand the structural integrity, retention of Keggin topology as well as crystallinity of the composite material. Accordingly, we conducted solid state ^{31}P -NMR for the HPW@Zr-BTC composites (18.6 and 28.2 wt%) to know the effect on the Keggin structure after encapsulation (Figure 8). One can find the literature chemical shift value for HPW i.e., -15.5 ppm, corresponding to the tetrahedral phosphorus, surrounded by wolfram octahedrae at the periphery [57]. The crests at -14.41 ppm for the 18.6 wt% HPW@Zr-BTC showed distortion of the Keggin topology due to stronger interactions with the host, and such trends were also reported by Kozhevnikov *et al.* [50] and Su *et al.* [20], independently. For 28.2 wt% HPW@Zr-BTC, the characteristic peak at -16.35 ppm was noticed, which was referred to the tetrahedral $[\text{PO}_4]^{4-}$ in the Keggin structure. The slight deviation from the mean value reflected to the fact that the Keggin structure was retained yet interactive with the host matrix [19,20]. The shoulder peak at -14.87 ppm for 28.2 wt% sample showed the stronger interaction of the support with the heteropoly anions [48]. These findings were also corroborated by XPS results (*vide supra*).

4 Catalytic tests

The catalytic activity of the HPW@Zr-BTC composite was adequately explored by Friedel-Crafts acylation of anisole with benzoyl chloride as an acylating agent in line with Scheme 2. All reactions were undertaken in liquid phase batch reactor at 120 °C and at atmospheric pressure for 6 h under constant stirring with anisole to benzoyl chloride (BoC) molar ratio 1:2, respectively. The major product obtained was *p*-methoxybenzophenone (yield~98%), while *o*-methoxybenzophenone was produced as minor product (Table 2). With pristine Zr-BTC, the anisole conversion was only 37.77%, whereas the HPW@Zr-BTC composites showed excellent activity, owing to the availability of strong active sites. The 28.2 wt% HPW@Zr-BTC gave best results amongst all the hybrid catalysts employed giving 99.4% anisole conversion. Furthermore, the low HPW loaded sample, i.e., 18.6 wt% gave merely 68% conversion which sequentially increased with the increase in the HPW content, due to availability of more active sites (Figure 9). In addition to this, it was observed that the catalytic activity of 32.2 wt% HPW@Zr-BTC was lesser than its 28.2 wt%, which might be due to pore blockage by HPW, as revealed by BET surface area and pore size distribution (Figure 4). Such trends have also been reported by Lingaiah *et al.* [19] and by Ammar *et al.* [49]. The possible structural representation and catalysis of the hybrid material are shown in Scheme 3, also proposed by Su *et al.* [20] for their HPW supported ZrO_2 .

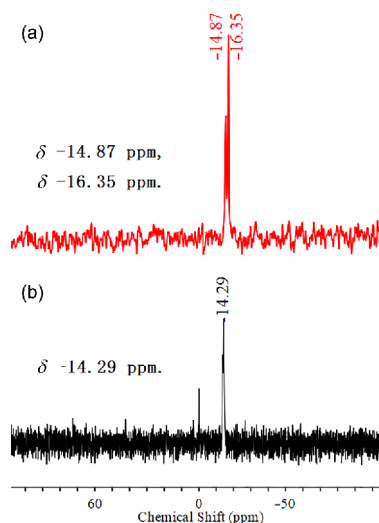
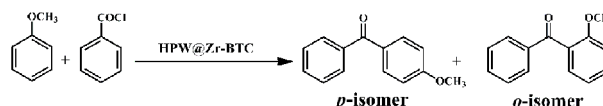
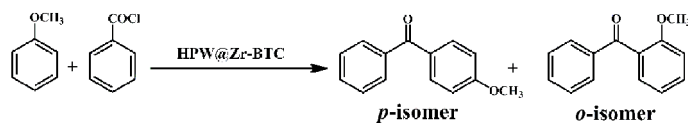


Figure 8 Solid state of ^{31}P -NMR 18.6 wt% HPW@Zr-BTC (a) and 28.2 wt% HPW@Zr-BTC (b) (color online).



Scheme 2 Anisole acylation with benzoyl chloride.

Table 2 Reaction inferences of 28.2 wt% HPW@Zr-BTC catalyzed anisole acylation^{a)}

Entry	Catalyst content (wt%)	HPW content (wt%)	Zr-BTC content (wt%)	Conversion (%)	Yield (%)
1	1.5	0.429	1.071	37.77	34.01
2	3.0	0.858	2.142	72.76	67.05
3	4.5	1.287	3.213	83.07	78.43
4	6.0	1.716	4.284	91.87	87.8
5	7.5	2.145	5.355	96.36	94.92
6	8.0	2.288	5.712	99.37	97.96

a) Reaction conditions: anisole to BoC molar ratio 1:2 moles, 120 °C for 6 h.

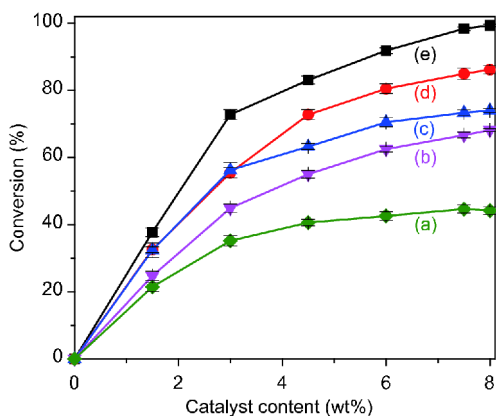


Figure 9 Catalytic activity of pristine Zr-BTC (a), 18.6 wt% HPW@Zr-BTC (b), 25.2 wt% HPW@Zr-BTC (c), 32.2 wt% HPW@Zr-BTC (d), and 28.2 wt% HPW@Zr-BTC (e) (Reaction conditions: anisole to BoC molar ratio 1:2 moles, temperature 120 °C, time 6 h) (color online).

5 Optimization of reaction variables

5.1 Effect of catalyst amount

It is reported that Friedel-Crafts acylation requires an extra stoichiometric amount of acid catalyst due to complexation with the oxygen atoms [58]. This extra catalyst consumption caused cost ineffectiveness vis-à-vis inevitable environmental risks. As shown in Table 2, the amount of catalyst significantly affects the rate of reaction, i.e., 34% to 99.4% conversion observed from 1.5 to 8.0 wt% for the 28.2 wt% HPW@Zr-BTC in a relatively shorter reaction time. Further increase in the catalyst amount had no significant effect upon anisole conversion. Earlier studies reported different catalyst for anisole acylation (Table 3), like AIPW₁₂O₄₀ could give 94% yield with benzoyl chloride [49]. Ammar *et al.* [49] reported 94.5% yield, for the same reaction with dodecaphosphotungstic acid encapsulated in ZIF-67 metal-organic framework. In another work, the selectivity of *p*-isomer was reported to be 90% for the H-Beta type zeolites previously

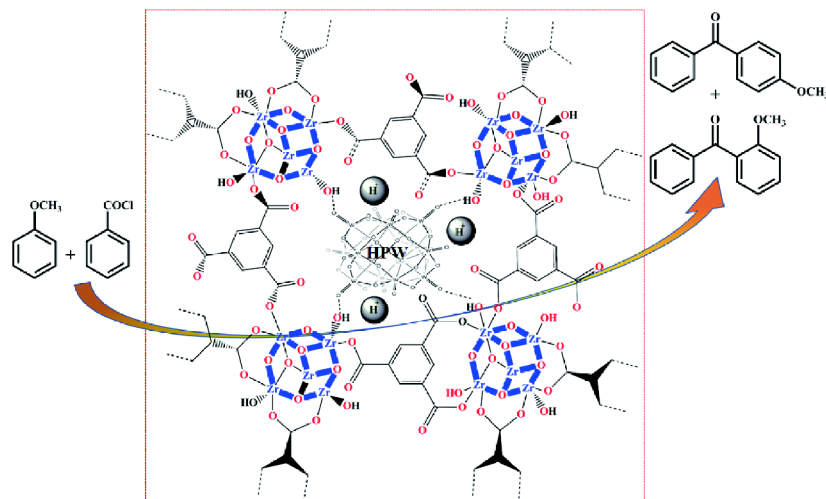
modified with Ga and In chloride/oxide [60]. Patil *et al.* [61] claimed 95% selectivity for their borate zirconia catalyst. In connection to these results, the bulk HPW gave 100% conversion in our study, but lower yield for the para isomer due to over oxidation and formation of methyl/phenyl benzoates, besides we were unable to recover HPW after the reaction. Henceforth, the promising yield (~98%) for the FC acylation of anisole with benzoyl chloride, show the competitiveness of the 28.2 wt% HPW@Zr-BTC hybrid catalyst against the reported and conventional catalytic systems.

5.2 Effect of reaction temperature

Since temperature plays a vital role in any chemical reaction, we subsequently investigated the effect of temperature in our system from 100, 110, 120, 130 and 140 °C. It was found that the optimum temperature for this reaction was 120 °C (Figure 10). Further increase in reaction temperature did not reveal any significant change on the anisole conversion due to establishment of reaction equilibria. However, decrease in reaction temperature greatly affected the course of reaction. At 100 °C, only 45% conversion and 86% selectivity were observed as compared to 72% conversion and 92.3% selectivity at 110 °C and 99.4% conversion 98.5% selectivity at 120 °C. Further increase to 130 and 140 °C resulted in small rise in the conversion at the expense of selectivity due to the formation of etheric side products.

5.3 Re-usability of the catalyst

The re-usability of a catalyst is of prime importance, consequently HPW@Zr-BTC catalyst was investigated for its re-usability and ease of separation from the reaction media. After the completion of a typical reaction (Sect. 4), the catalyst was removed by simple centrifugation (7000 r/min for 5 min), washed with dichloromethane to remove traces of adsorbed reagents and dried overnight at 60 °C before acti-



Scheme 3 Schematic representations of HPW interaction with the Zr-BTC host: catalyst for anisole acylation (color online).

Table 3 Anisole acylation with benzoyl chloride by different catalysts (comparison)

Entry	Catalyst type	Catalyst content (wt%)	An ^{c)/} BoC ^{d)} (mol/mol)	Tempture (°C)	Yield (%)
1	28.2 wt% HPW@Zr-BTC	8	0.5	120	97.9 ^{b)}
2	Zr-BTC	8	0.5	120	25.5 ^{b)}
3	HPW	8	0.5	120	96.7 ^{b)}
4	H-beta	8	0.5	120	65.5 ^{b)}
5	H-Beta	20	0.8	150	92.8 [61]
6	26.5wt% PTA@ZIF-67	10	0.5	120	94.5 [49]
7	AIPW ₁₂ O ₄₀	4	0.6	60-70	94.0 [59]
8	20% In ₂ O ₃ -HP ^{a)}	20	2.0	80	90.0 [60]
9	B ₂ O ₃ /ZrO ₂ ^{a)}	20	0.8	150	87.8 [61]

a) Nitrobenzene as solvent; b) this study; c) an-anisole; d) BoC-benzoyl chloride.

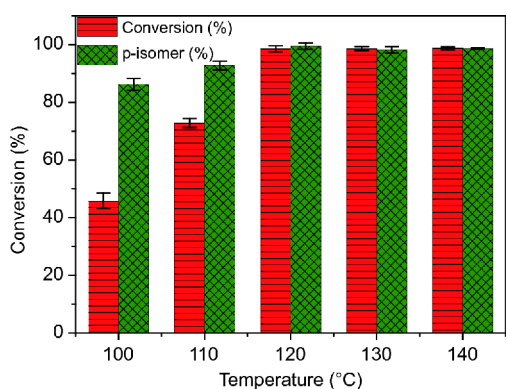


Figure 10 Temperature effect upon the catalytic activity of 28.2 wt% HPW@Zr-BTC (reaction conditions: anisole to BoC molar ratio 1:2, reaction time 6 h) (color online).

vation at 110 °C for 6 h. It was observed that the catalyst was easily separable from the reaction medium, showing the heterogeneity of the catalyst. In this way the spent 28.2 wt% HPW@Zr-BTC catalyst was applied in at least 5 consecutive

runs giving 99.4%, 92.7%, 92.1%, 90.5% and 89.2% conversion under the same reaction conditions (within experimental error) (Figure 11).

5.4 Catalyst leaching tests

Leaching of heteropoly acids into the reaction media is the bottleneck to their applicability on larger scale. To confirm whether the active material had leached into the reaction medium or not, controlled test reactions were carried out. Here, the reaction assembly as previously described was split into two parts after 4 h on the reaction. One part was run undisturbed, while the second part was filtered to remove the solid catalyst particles, and the reaction was carried out keeping the other reaction conditions same. As shown in Figure 12, the part which had been filtered has stopped further reacting, which proved that the catalyst HPW@Zr-BTC was robust and resistant to leaching. To further validate these findings, inductively coupled plasma (ICP) analyses were done to determine the tungsten traces in the reaction

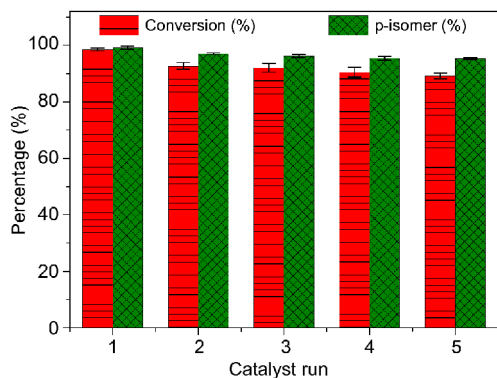


Figure 11 Catalyst re-usability for 28.2 wt% HPW@Zr-BTC (Reaction conditions: anisole to BoC molar ratio 1:2 moles, temperature 120 °C, time 6 h) (color online).

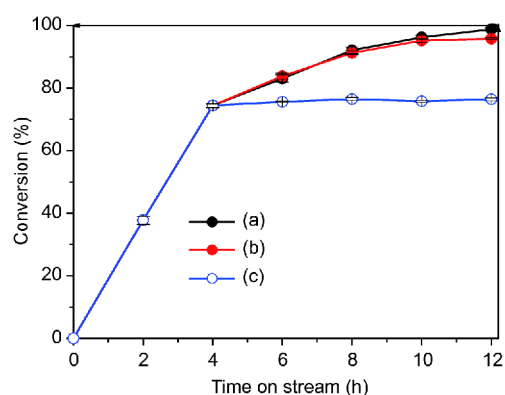


Figure 12 Catalyst leaching tests for anisole acylation using 28.2 wt% HPW@Zr-BTC at 120 °C for 12 h. (a) 1st run, (b) 2nd run, (c) catalyst filtered (Reaction conditions: anisole to BoC molar ratio 1:2) (color online)

media. Here, the whole reaction assembly was dried in a china dish, followed by dissolution (whatever the remainder) in nitric acid and tested for tungsten traces using ICP-OES. No tungsten traces were observed, which unequivocally confirmed the robustness of the structure and permanency of the guest HPW inside the Zr-BTC host.

6 Conclusions

Zr-BTC (metal-organic framework) owing to its resilient nature, non-hazardous metal edifice, large surface area, and appropriate pore dimensions was studied to act as a potential host for the heteropoly acids. Dodeca-tungstophosphoric acid ($H_3PW_{12}O_{40}$) was snugly caged (with varied ratios up to a maximum of 32.3 wt%) inside the microspores of Zr-BTC by one pot solvothermal method, and thoroughly characterized by advanced elucidation techniques. Heteropoly anions, were shown to stabilize the structure of metal-organic framework, likely due to their anionic templating effect. The prepared HPW@Zr-BTC composites had re-

silient catalytic sites as revealed by anisole acylation, with 28.2 wt% HPW@Zr-BTC showed the best catalytic results (anisole conversion 99.4%). No leaching and hence no obvious reduction in catalytic activity was observed during five consecutive runs, which indicated the permanency of HPW guest inside the Zr-BTC framework host.

Acknowledgements This work was supported by the National Key Research and Development Program of China (2016YFB0601303), the National Natural Science Foundation of China (51374193, 21676278), Key Program of National Natural Science Foundation of China (9143420), and Chinese Academy of Sciences, State Administration of Foreign Experts Affairs (CAS/SAFEA) International Partnership Program for Creative Research Teams (20140491518). Latif Ullah acknowledged the Chinese Academy of Sciences (CAS) and the World Academy of Sciences (TWAS) for providing with the opportunity to pursue research work under the umbrella of CAS-TWAS Presidents' Fellowship.

Conflict of interest The authors declare that they have no conflict of interest.

Supporting information The supporting information is available online at <http://chem.scichina.com> and <http://link.springer.com/journal/11426>. The supporting materials are published as submitted, without typesetting or editing. The responsibility for scientific accuracy and content remains entirely with the authors.

- Okuhara T. *Chem Rev*, 2002, 102: 3641–3666
- Usman M, Li D, Li CS, Zhang SJ. *Sci China Chem*, 2015, 58: 738–746
- Wang SS, Yang GY. *Chem Rev*, 2015, 115: 4893–4962
- Mizuno N, Misono M. *Chem Rev*, 1998, 98: 199–218
- Wang J, Zhao J, Niu J, Guo D, Dang D. *Sci China Ser B*, 2003, 46: 583–594
- Zhou L, Wang L, Zhang S, Yan R, Diao Y. *J Catal*, 2015, 329: 431–440
- Campos-Martin JM, Capel-Sanchez MC, Fierro JLG. *Green Chem*, 2004, 6: 557–562
- Lv H, Geletii YV, Zhao C, Vickers JW, Zhu G, Luo Z, Song J, Lian T, Musaei DG, Hill CL. *Chem Soc Rev*, 2012, 41: 7572–7589
- Liu R, Shang X, Li C, Xing X, Yu X, Zhang G, Zhang S, Cao H, Bi L. *Int J Hydrogen Energy*, 2013, 38: 9954–9960
- Zhang H, Yan R, Yang L, Diao Y, Wang L, Zhang S. *Ind Eng Chem Res*, 2013, 52: 4484–4490
- Xing X, Wang M, Liu R, Zhang S, Zhang K, Li B, Zhang G. *Green Energy Environ*, 2016, 1: 138–143
- Zheng Y, Zhang H, Wang L, Zhang S, Wang S. *Front Chem Sci Eng*, 2016, 10: 139–146
- Kozhevnikov IV. *Chem Rev*, 1998, 98: 171–198
- Gouzerh P, Proust A. *Chem Rev*, 1998, 98: 77–112
- Liu C, Zhang Z, Liu W, Du X, Liu S, Cui Y. *Green Energy Environ*, 2017, 2: 436–441
- Romanelli G, Autino JC, Vázquez P, Pizzio L, Blanco M, Cáceres C. *Appl Catal A*, 2009, 352: 208–213
- Ferreira P, Fonseca IM, Ramos AM, Vital J, Castanheiro JE. *Catal Commun*, 2011, 12: 573–576
- Blasco T, Corma A, Martínez A, Martínezescolano P. *J Catal*, 1998, 177: 306–313
- Kumar C R, M. S, Lingaiah N. *Appl Catal A*, 2014, 487: 165–171
- Su F, Ma L, Guo Y, Li W. *Catal Sci Technol*, 2012, 2: 2367–2374
- Li H, Eddaoudi M, O'Keeffe M, Yaghi OM. *Nature*, 1999, 402: 276–279
- Wu L, Xue M, Huang L, Qiu SL. *Sci China Chem*, 2011, 54: 1441–

- 1445
- 23 James SL. *Chem Soc Rev*, 2003, 32: 276–288
- 24 Férey G, Mellot-Draznieks C, Serre C, Millange F, Dutour J, Surlblé S, Margiolaki I. *Science*, 2005, 309: 2040–2042
- 25 Sun CY, Liu SX, Liang DD, Shao KZ, Ren YH, Su ZM. *J Am Chem Soc*, 2009, 131: 1883–1888
- 26 Maksimchuk N, Timofeeva M, Melgunov M, Shmakov A, Chesalov Y, Dybtsev D, Fedin V, Kholdeeva O. *J Catal*, 2008, 257: 315–323
- 27 Wang XS, Huang YB, Lin ZJ, Cao R. *Dalton Trans*, 2014, 43: 11950–11958
- 28 Bromberg L, Diao Y, Wu H, Speakman SA, Hatton TA. *Chem Mater*, 2012, 24: 1664–1675
- 29 Juan-Alcañiz J, Gascon J, Kapteijn F. *J Mater Chem*, 2012, 22: 10102–10118
- 30 Yu R, Kuang XF, Wu XY, Lu CZ, Donahue JP. *Coordin Chem Rev*, 2009, 253: 2872–2890
- 31 Canioni R, Roch-Marchal C, Sécheresse F, Horcajada P, Serre C, Hardi-Dan M, Férey G, Grenèche JM, Lefebvre F, Chang JS, Hwang YK, Lebedev O, Turner S, Van Tendeloo G. *J Mater Chem*, 2011, 21: 1226–1233
- 32 Xiao B, Wheatley PS, Zhao X, Fletcher AJ, Fox S, Rossi AG, Megson IL, Bordiga S, Regli L, Thomas KM, Morris RE. *J Am Chem Soc*, 2007, 129: 1203–1209
- 33 Jiang J, Gándara F, Zhang YB, Na K, Yaghi OM, Klemperer WG. *J Am Chem Soc*, 2014, 136: 12844–12847
- 34 Cavka JH, Jakobsen S, Olsbye U, Guillou N, Lamberti C, Bordiga S, Lillerud KP. *J Am Chem Soc*, 2008, 130: 13850–13851
- 35 Piscopo CG, Polyzoidis A, Schwarzer M, Loebbecke S. *Micropor Mesopor Mater*, 2015, 208: 30–35
- 36 Zhou F, Lu N, Fan B, Wang H, Li R. *J Energy Chem*, 2016, 25: 874–879
- 37 Salomon W, Roch-Marchal C, Mialane P, Rouschmeyer P, Serre C, Haouas M, Taulelle F, Yang S, Ruhlmann L, Dolbecq A. *Chem Commun*, 2015, 51: 2972–2975
- 38 Yang XL, Qiao LM, Dai WL. *Micropor Mesopor Mater*, 2015, 211: 73–81
- 39 Misono M, Mizuno N, Katamura K, Kasai A, Konishi Y, Sakata K, Okuhara T, Yoneda Y. *Bull Chem Soc Jpn*, 1982, 55: 400–406
- 40 Olah GA, Reddy VP, Prakash GKS. *Friedel-Crafts Reactions*. New York: John Wiley & Sons, Inc., 2000. 159–199
- 41 Qiu R, Chen Y, Yin SF, Xu X, Au CT. *RSC Adv*, 2012, 2: 10774–10793
- 42 Dhakshinamoorthy A, Opanasenko M, Čejka J, Garcia H. *Catal Sci Technol*, 2013, 3: 2509–2540
- 43 El-Hiti GA, Smith K, S. Hegazy A. *Curr Org Chem*, 2015, 19: 585–598
- 44 Furukawa H, Gándara F, Zhang YB, Jiang J, Queen WL, Hudson MR, Yaghi OM. *J Am Chem Soc*, 2014, 136: 4369–4381
- 45 Schaate A, Roy P, Godt A, Lippke J, Waltz F, Wiebcke M, Behrens P. *Chem Eur J*, 2011, 17: 6643–6651
- 46 Kholdeeva OA, Maksimov GM, Maksimovskaya RI, Vanina MP, Trubitsina TA, Naumov DY, Kolesov BA, Antonova NS, Carbó JJ, Poble JM. *Inorg Chem*, 2006, 45: 7224–7234
- 47 Vanhaecht S, Absillis G, Parac-Vogt TN. *Dalton Trans*, 2013, 42: 15437–15446
- 48 Xu X, Lu Y, Yang Y, Nosheen F, Wang X. *Sci China Mater*, 2015, 58: 370–377
- 49 Ammar M, Jiang S, Ji S. *J Solid State Chem*, 2016, 233: 303–310
- 50 Kozhevnikov IV, Sinnema A, Jansen RJJ, Pamin K, van Bekkum H. *Catal Lett*, 1994, 30: 241–252
- 51 Rocchiccioli-Deltcheff C, Fournier M, Franck R, Thouvenot R. *Inorg Chem*, 1983, 22: 207–216
- 52 Thielemann JP, Girgsdies F, Schlögl R, Hess C. *Beilstein J Nanotechnol*, 2011, 2: 110–118
- 53 Khyzhun OY. *J Alloys Compd*, 2000, 305: 1–6
- 54 Morris RE WP. Adsorption and release of nitric oxide in metal-organic frameworks. US Patent, 8486451, 2010-09-23
- 55 Wee LH, Wiktor C, Turner S, Vanderlinden W, Janssens N, Bajpe SR, Houthoofd K, Van Tendeloo G, De Feyter S, Kirschhock CEA, Martens JA. *J Am Chem Soc*, 2012, 134: 10911–10919
- 56 Li SW, Gao RM, Zhang RL, Zhao J. *Fuel*, 2016, 184: 18–27
- 57 Okuhara T, Watanabe H, Nishimura T, Inumaru K, Misono M. *Chem Mater*, 2000, 12: 2230–2238
- 58 de Noronha RG, Fernandes AC, Romão CC. *Tetrahedron Lett*, 2009, 50: 1407–1410
- 59 Firouzabadi H, Iranpoor N, Nowrouzi F. *Tetrahedron*, 2004, 60: 10843–10850
- 60 Choudhary VR, Jana SK, Patil NS, K. Bhargava S. *Micropor Mesopor Mater*, 2003, 57: 21–35
- 61 Patil PT, Malshe KM, Kumar P, Dongare MK, Kemnitz E. *Catal Commun*, 2002, 3: 411–416